

1 *Revision 2 (#5614) – Submitted to American Mineralogist*

2

3 Morphological and chemical evolution of corundum (ruby and sapphire):

4 crystal ontogeny reconstructed by EMPA, LA-ICP-MS and Cr³⁺ Raman

5 mapping

6

7 ELENA S. SOROKINA^{1,2} (CORRESPONDING AUTHOR, E-MAIL:

8 ELENA.SOROKINA@GIA.EDU), WOLFGANG HOFMEISTER³, TOBIAS

9 HÄGER³, REGINA MERTZ-KRAUS³, STEFAN BUHRE³, AND JOHN M.

10 SAUL⁴

11 ¹ Gemological Institute of America, 5355 Armada Dr, Carlsbad, California,
12 92008, United States of America;

13 ² Fersman Mineralogical Museum of the Russian Academy of Sciences (RAS),
14 Leninskiy prosp., 18 b. 2, Moscow, 119071, Russia;

15 ³ Institute for Geosciences of the Johannes Gutenberg-University Mainz (JGU),
16 J.-J.-Becher-Weg 21, D-55128 Mainz, Germany

17 ⁴ Swala Gem Traders, Box 11063, Arusha, Tanzania

18

19 **ABSTRACT**

20 The term “*ontogeny*”, which is commonly used in biology, was introduced

21 into the earth sciences in 1961 to include the genesis and evolution of single

22 crystals and crystal aggregates. The term encompasses *nucleation*, *growth*,
23 *alteration*, and *destruction*. We present results of studies concerning the
24 ontogeny of natural corundum (rubies and sapphires), and the chemical and
25 morphological evolution of corundum crystals from deposits in Africa (Kenya,
26 Tanzania, Madagascar) and Southeast Asia (Vietnam). Trace-element
27 compositions indicative for different corundum habits were determined by rim-
28 to-rim LA-ICP-MS and EMPA analyses. Raman spectroscopy was applied for
29 Cr³⁺ photoluminescence mapping. Results traced the development of corundum
30 crystals and the evolution of their chemistry and morphology, and helped to
31 clarify the geological processes within particular deposits. These variations of
32 corundum morphology are directly correlated with Cr and Fe contents and
33 varying P-T conditions that prevailed during crystal growth. Dipyramidal habits
34 combined with white color in corundum from two deposits in the Mangari area
35 in Kenya have Cr concentrations of ~ 200 - 700 µg/g in crystals that grew under
36 high P-T conditions. Prismatic habit of bright red ruby crystals was linked to Cr
37 concentrations of ≥1500 µg/g in samples from Luc Yen (Vietnam) and Mangari
38 (Kenya), formed under lower P-T. Concentrations of Cr between 700–1500
39 µg/g are associated with pink color and combinations of different habits
40 (dipyramidal, prismatic, or dipyramidal-prismatic) in these samples. Contents
41 of Fe ~700 µg/g and Cr ~1200 µg/g in sapphire crystals from the Morogoro

42 area of Tanzania caused pink color that correlated with dipyramidal habit and
43 elongation along the c axis. Rhombohedral habit and blue-violet color were
44 observed at Cr \sim 600 $\mu\text{g/g}$ and Fe \geq 2000 $\mu\text{g/g}$ in sapphires from
45 Andranondambo in Madagascar, formed during the final stage of contact
46 metamorphism.

47 **Keywords:** Corundum, ruby, sapphire, ontogeny, evolution, genesis,
48 geochemistry, crystal morphology, Kenya, Tanzania, Madagascar, Vietnam.

49

72 1979; Pirogov, 1985; Pavlishin et al., 1988; Prieto et al., 1992; Self and Hill,
73 2003; Sorokina, 2011; Alekseev and Marin, 2012; Sorokina et al., 2012 etc.).
74 Evolutionary direction in the proliferation of mineral species has been proposed
75 and discussed by Hazen et al. (2008) and Krivovichev (2013).

76 This article presents results on the evolution of morphology and changing
77 geochemistry of opaque and transparent corundum crystals during growth and
78 alteration for samples from five important deposits in Africa (Mangari area in
79 Kenya, Morogoro in Tanzania, and Andranondambo in Madagascar) and
80 Southeast Asia (Luc Yen in Vietnam). Rim-to-rim chemical analyses were
81 combined with Cr³⁺ photoluminescence mapping for corundum with visual
82 color zoning from Mangari. This allowed *in-situ* observations of the distribution
83 of Cr³⁺ content within the mineral matrix.

84 In the past, rim-to-rim ion probe analyses on Scottish sapphires were
85 combined with cathodoluminescence in a study by Upton et al. (1999), and
86 color zoning in Myanmar rubies were investigated by electron microprobe
87 analysis (EMPA), Laser Ablation-Inductively Coupled Plasma-Mass
88 Spectrometry (LA-ICP-MS) and cathodoluminescence elemental mapping by
89 Harlow and Bender (2013), and by Zaw et al. (2015). However those studies
90 did not directly address corundum crystal habit. We determined concentrations
91 of trace elements V, Cr, Fe, Ti, Ga and Mg, which may associate with particular

92 crystal habits. Trace element results on Kenyan ruby (Acharya et al., 1997;
93 Mulmeister et al., 1998) were less detailed and less concerned with crystal
94 habits than this study. To the best of our knowledge, our work on corundum
95 from Kenya is new; for other deposits, we update geochemical data using a
96 combination of EMPA and LA-ICP-MS analyses. Chemical composition of
97 corundum during growth was correlated with the changes of crystallization
98 parameters (in particular, P-T conditions) obtained from the literature, thereby
99 allowing us to reconstruct the development of crystals.

100

MATERIALS AND METHODS

101 Transparent and opaque samples of naturally occurring corundum of
102 different colors and morphologies were selected along with their host rocks
103 from the collections of the Institute for Geosciences in the Johannes Gutenberg-
104 University Mainz (Figure 1). Our samples came from a marble-hosted deposit
105 near Morogoro in Tanzania (2 samples), the Gitonga pit of the John Saul ruby
106 mine in the Mangari area of Kenya (9 samples), the Aqua ruby mine (formerly
107 part of the Penny Lane mine) also in the Mangari area (1 sample), the
108 Andranondambo skarn deposit of Madagascar (4 samples), the Luc Yen
109 marble-hosted primary deposit in Vietnam (2 samples), and a secondary
110 occurrence from the Luc Yen area (1 sample).

111 In order to study microscopic features of these corundum crystals, macro-
112 and micro-scale observations were made using a Zeiss Stemi SV11 stereo zoom
113 microscope with a horizontal arrangement. Parts of rocks containing transparent
114 crystals of corundum (ruby and sapphire) were dissolved in 30 % HCl and 30 %
115 HF and/or mechanically crushed to separate the crystals from their matrix.
116 Representative corundum crystals were cut into plates perpendicular and
117 parallel to the *c* axis in order to facilitate the study of internal features appearing
118 in different crystallographic directions.

119 Rim-to-rim chemical profiles of corundum samples differently orientated
120 with respect to the *c* axis were investigated at the laboratories of the Johannes
121 Gutenberg-University Mainz using EMPA and LA-ICP-MS.

122 JEOL JXA 8200 electron microprobe in the wavelength-dispersive
123 detection mode was used in the following operating conditions: 20 kV
124 acceleration voltage, 20 nA beam current, 20 s peak counting times for Al; 80 s
125 for Si; 100 s for Ti, Cr, Mn and Fe; 200 s for V and Ga, with a spot size of 3
126 μm . Sets of natural and synthetic reference materials were used for calibration
127 and instrument-stability monitoring: Al_2O_3 for Al, Cr_2O_3 for Cr, Fe_2O_3 for Fe,
128 GaAs for Ga, MgO for Mg, MnTiO_3 for Mn and Ti, metallic V for V, and
129 wollastonite for Si. An overlap correction was applied for $\text{Ti} > \text{V}$ and $\text{V} > \text{Cr}$.
130 The detection limits for measured elements varied for different analytical

131 sessions: Ti 60 $\mu\text{g/g}$, V 118 – 446 $\mu\text{g/g}$, Ga 132 – 472 $\mu\text{g/g}$, Fe 74 – 76 $\mu\text{g/g}$, Cr
132 220 – 370 $\mu\text{g/g}$, Mn 58 – 224 $\mu\text{g/g}$, and Mg 90 – 256 $\mu\text{g/g}$.

133 LA-ICP-MS measurements were made along profiles situated parallel to the
134 EMPA profiles using an ESI NWR193 ArF Excimer Laser combined with an
135 Agilent 7500ce quadrupole-ICP-MS. Analyses were carried out with a spot size
136 of 70 μm at a repetition rate of 10 Hz and an energy density of approximately
137 3.0 J/cm^2 . Warm-up/background time was 15 s, dwell time 30 s, and wash out
138 time 20 s. NIST SRM 612 was used as reference material for calibration,
139 applying the preferred values for NIST SRM 612 in the GeoReM database,
140 <http://georem.mpch-mainz.gwdg.de/> (Jochum et al., 2005, 2011), as the “true”
141 concentrations in calculating the element values within the samples.
142 Additionally, we analyzed NIST SRM 610 and basaltic USGS BCR-2G as
143 quality control materials (QCM) several times during each analytical sequence.
144 The time-resolved signal was processed using the program GLITTER 4.4.1
145 (www.glitter-gemoc.com, Macquarie University, Sydney, Australia) using ^{27}Al
146 as the internal standard, applying the Al_2O_3 content previously determined by
147 EMPA for the corundum samples and the values reported in the GeoReM
148 database for the QCM. The measured concentrations for both QCM agree for
149 most elements within 15 % with the preferred values provided in the GeoReM
150 database. Measured average concentrations for Cr for BCR-2G are too low by

151 23 %. This larger discrepancy between measured and preferred values can be
152 attributed to isobaric interferences that cannot be resolved with the
153 instrumentation used (Jochum et al. 2012). For the QCM, the relative standard
154 deviation for the average concentrations determined was always <7%. Average
155 detection limits were calculated from measurements on the reference materials:
156 Mg 2.2 µg/g, Ti 3.8 µg/g, V 0.2 µg/g, Mn 1.0 µg/g, Ga 0.2 µg/g, Cr 3.2 µg/g.
157 Due to the large number of possible interferences on Fe in an argon-oxygen
158 atmosphere, concentrations for this element are reported only by EMPA data.

159 In order to monitor the distribution of chromium within Mangari corundum
160 crystals with visual color oscillatory zoning, Cr³⁺ luminescence mapping was
161 acquired. A confocal Raman Spectrometer (RS) made by Horiba Yobin Yvon
162 HR800 was coupled with an Olympus BX41 microscope and automatic XYZ-
163 stage with the mapping technique. Red helium-neon laser with $\lambda = 633$ nm
164 (polarized during the measurements) was used with a grating of 1800
165 grooves/mm. The confocal hole of 400 µm and the entrance slit of 100 µm
166 produce a resolution of 0.7 (blue) to 0.5 (red) cm⁻¹ for an exposition time of 0.5
167 s with measured steps of 100 µm. Magnification x50 was used for measured
168 range of 697.0 – 709.0 nm. Relative chromium contents were determined using
169 the peak-ratio of the n-line peak at about 701.55 nm with the side-band peak at

170 about 707.2 nm (Häger & Dung, 2000). The spectrometer was calibrated at
171 520.7 cm^{-1} using Si as a reference.

172 LOCAL GEOLOGY

173 The corundum deposits in *Luc Yen* and Yen Bai areas of northern Vietnam
174 are located in the Lo Gam tectonic zone, on the northeastern side of the Red
175 River shear zone (Hoang Quang et al., 1999; Pham Van et al., 2004 and
176 references therein). Crystallization took place along the retrograde metamorphic
177 path at 630 – 670 °C and 2.9 – 3.3 kbar (Garnier et al., 2005). Mineral
178 associations in samples from the primary Luc Yen marble-hosted deposit
179 include bright red ruby, fuchsite, blue micas, muscovite, and pyrrhotite,
180 cemented by well-formed calcite crystals. Elongate-prismatic ruby crystals with
181 z ($22\bar{4}1$), ω ($14\ 14\ \bar{2}8\ 3$), n ($22\bar{4}3$), c (0001), and r ($10\bar{1}1$) faces are arranged
182 randomly in the host calcite matrix, sporadically intergrown with green and
183 blue micas (Fig. 1A). Dravite, phlogopite, rutile, spinel, edenite, and graphite
184 were also observed (Pham Van et al., 2004). Secondary Luc Yen deposits
185 consist of gravel in karst pockets and alluvial fans (Kane et al., 1991). Our
186 secondary samples include elongate-prismatic crystals of corundum with
187 z ($22\bar{4}1$), ω ($14\ 14\ \bar{2}8\ 3$), n ($22\bar{4}3$), c (0001), and r ($10\bar{1}1$) faces and elongate
188 dipyramidal crystals with c (0001) and ω ($14\ 14\ \bar{2}8\ 3$) faces. Colors include
189 pink, purple to red, and yellowish-red. Such crystals are associated with

190 fuchsite, calcite relicts, and secondary clay minerals formed as a result of
191 calcite marble replacement. Cubic crystals of hematite replacing pyrite are also
192 present. Some of the ruby crystals are cemented in disorderly fashion to one
193 another by clay minerals forming masses resembling druse-like aggregates (Fig.
194 1B). Other researchers (e.g., Kane et al., 1991) also described blue and colorless
195 sapphires coexisting with rubies, as well as grey to brown dipyramidal
196 sapphires and “trapiche” rubies. Red, pink, and pale blue spinel, gem quality
197 multi-color tourmaline, and garnet are also found.

198 The sapphire deposit to the south of the village of *Andranondambo*
199 (Tranomaro area, Madagascar) is derived from metamorphic skarn-type
200 deposits in the high-grade granulite facies of the Proterozoic Tranomaro Group,
201 composed of metapelites, calc-silicates, and marbles interlayered with
202 leucocratic gneiss (Rakotondrazafy et al., 1996). Three different metamorphic
203 stages were reported by Rakotondrazafy, et al. (2008). Minerals formed during
204 the first stage, a metasomatic event with $T \sim 850$ °C and $P \sim 5$ kbar, included
205 meionite, spinel, thorianite, and corundum within a titanite-bearing matrix of
206 scapolite and diopside. The second stage, also metasomatic, was characterized
207 by $T \sim 800$ °C and $P \sim 3\text{--}3.5$ kbar, and produced pargasite, anorthite, calcite,
208 phlogopite, and hibonite. Retrograde metamorphism followed with the
209 formation of gem blue sapphires at $T \sim 500$ °C and $P \sim 2$ kbar within K-feldspar

210 veins crosscutting marbles. Our samples show small-grained calcite and
211 dolomite, small grains of clinopyroxene, blue-violet sapphires with r ($10\bar{1}1$) and
212 a ($11\bar{2}0$) faces, and some pink sapphire crystals (Fig. 1C).

213 Corundum (ruby) deposits in the *Mangari* area (*John Saul, Aqua and Hard*
214 *Rock* mines) in the southeastern part of Kenya's Tsavo West National Park
215 have a metasomatic genesis produced during complex desilication of
216 pegmatites and ultrabasites (Simonet, 2000, Simonet et al., 2008). According to
217 Mercier et al. (1999), the ruby-bearing rocks were formed under granulite facies
218 conditions (700–750 °C, 8–10.5 kbar) in deeper crust and subsequently brought
219 up to their present level by the ultrabasic bodies during their emplacement as
220 thrust sheets. Corundum mineralization occurs in micaceous pockets within
221 serpentized ultrabasites and pegmatoid rock, as well as in veins crosscutting
222 the ultrabasites (Mercier et al., 1999). At the Aqua and Hard Rock mines,
223 transparent corundum in pockets is associated with phlogopite with lesser
224 muscovite, Mg-bearing chlorite, and Mg-bearing spinel. Corundum-bearing
225 veins are mainly composed of anorthite (An 95–98) and zoisite. At the John
226 Saul mine (which includes the Gitonga, Kimbo, Cowboy, and Main pits),
227 corundum occurs in lenses associated with plagioclase (An 18–26), muscovite,
228 Cr-bearing tourmaline, rutile, and graphite, and in layer-like pegmatite with
229 plagioclase (An 14–29), K-feldspar, muscovite, phlogopite, Cr-bearing

230 tourmaline, pyrite, and graphite. Materials used in this study also included
231 samples from the Aqua mine with the mineralogical association of small-
232 grained plagioclase (anorthite), corundum, and green mica (fuchsite) similar to
233 samples described by Mercier et al. (1999) for a corundum-bearing vein cutting
234 the ultrabasic body. Corundum crystals were zonal with different color.
235 Transparent bright red rims of elongate-prismatic form with z ($22\bar{4}1$),
236 $\omega(14\ 14\ \bar{2}8\ 3)$, n ($22\bar{4}3$), c (0001), and r ($10\bar{1}1$) faces are combined with
237 opaque white cores and intermediate areas with dipyrmidal faces (Fig. 1E).
238 Gitonga pit samples came to the collection as single crystals, and as white
239 clayey masses with corundum crystals encased by kaolinite and iron oxides
240 (Fig. 1D). In these samples, we also observed small blue mica plates
241 intergrowing with ruby crystals, small rutile grains, and star-like graphite
242 aggregates.

243 Corundum crystals (rubies and pink sapphires) from Central Tanzania, near
244 the town of *Morogoro*, were related to the Uluguru Mountains (Le Goff, 2004).
245 Corundum mineralization occurred at the contacts of biotite gneiss with marble
246 (Le Goff et al., 2008), with transparent red crystals (rubies) associated with
247 spinel and sapphirine. Their formation is caused by high-grade regional
248 metamorphism of a protolith of varied composition (Le Goff et al., 2004) at P
249 ~ 7.7 kbar and $T \sim 695$ °C, assuming $a_{\text{H}_2\text{O}} = 1$ (Alter et al., 1982). Our sample

250 is composed of elongate dipyrarnidal crystals of opaque pink sapphire with
251 $c(0001)$ and $\omega (14 14 \overline{28} 3)$ faces intergrown with fine-grained feldspar, plates
252 of biotite, rutile grains, and iron oxide minerals (fig. 1F).

253 RESULTS

254 Optical microscopy

255 Studied samples varied in color and have different internal features (Table
256 1). Transparent bright red material becomes visible in the marble-hosted
257 corundum from Luc Yen only after cutting plates parallel and perpendicular to
258 the c axis, but its distribution is not homogeneous and can vary from bright red
259 to reddish-pink within a single sample. A parting along $r (10\overline{1}1)$ faces is present
260 on these samples. Corundum crystals from the secondary deposit at Luc Yen
261 are fractured; their cores are transparent with bright red color and rims are
262 yellowish-red. In contrast, corundum crystals from the Mangari deposits in
263 Kenya (Aqua mine and the Gitonga pit of the John Saul mine) exhibit visual
264 oscillatory zoning even in unprepared samples: bright red transparent rims and
265 white-colored opaque cores are observable, with needle-like micro-inclusions
266 of rutile along growth faces in the intermediate area between rim and core. A
267 pink corundum sample from the Morogoro area (Tanzania) is completely
268 opaque. The bright pink, blue-violet and grey-blue sapphires from

269 Andranondambo (Madagascar) are transparent and show parting along r ($10\bar{1}1$)
270 faces.

271

272 **Rim-to-rim LA-ICP-MS and EMPA traverses, and RS Cr³⁺ mapping**

273 Changes of crystal chemistry and crystal morphology were observed in
274 corundum samples cut into plates orientated differently with respect to the c
275 axis. Determinations were made by rim-to-rim micro-chemical analyses using
276 EMPA and LA-ICP-MS with spacing of 800 – 1000 μm between spots (Table
277 1).

278 Differences in concentrations determined by the two methods were
279 relatively minor and are attributed to inhomogeneous element distribution in the
280 corundum matrix. EMPA and LA-ICP-MS profiles are offset by some μm and
281 the different beam diameters of EMPA ($\sim 3 \mu\text{m}$) and LA-ICP-MS ($\sim 70 \mu\text{m}$)
282 result in target larger areas for the LA-ICP-MS analyses. Differences in
283 operation conditions and their effects on concentrations obtained by EMPA and
284 LA-ICP-MS were previously observed by Zaw et al., 2015. Due to the absence
285 of well-characterized reference materials with a corundum matrix, calibration of
286 the LA-ICP-MS measurements was performed using synthetic silicate glass
287 reference material. This non-matrix matched calibration influences the accuracy
288 of the determined element concentrations, as demonstrated, for instance, by the

289 deviation of Cr in BCR-2G from its preferred value. For the EMPA
290 measurements 2 sigma uncertainties of up to 20 % have to be considered for the
291 trace elements due to low concentrations and calibration using non-oxide
292 standards (*e.g.* GaAs for Ga). Differences in values for Cr (x1.25 to x1.7) and
293 for Ga (x1.4) – as determined by the two methods in several spots on samples
294 from Luc Yen, Morogoro, Gitonga pit, Aqua mine, and Andranondambo – can
295 be related to the reasons mentioned above, but in addition, the ablation of
296 inclusions in those samples is also a likely source of discrepancies, particularly
297 as regards Ti. LA-ICP-MS values for Ti in some spots measured on Luc Yen,
298 Morogoro, Gitonga pit, and Aqua mine corundums are 1.6 – 2.8 times higher
299 than their respective EMPA values, and up to 16 times higher in some points on
300 a Gitonga pit sample. This is attributed to the ablation of corundum material
301 containing titanium dioxide (rutile) micro-inclusions. Figure 2 shows visual
302 oscillatory zoning in Gitonga pit corundums caused by the distribution of
303 needle-like rutile micro-inclusions along the corundum growth faces.

304 Studies of corundum crystals from the Aqua mine and from the Gitonga pit,
305 both Mangari deposits (Kenya), have shown that the crystal habit changed from
306 dipyramidal nearly opaque cores with white color in the beginning of growth to
307 prismatic red transparent rims in the end. These changes during crystal growth
308 correspond to the increase of Cr concentration from around 200 µg/g in core to

309 more than 1500 $\mu\text{g/g}$ in the rim (Fig. 2). Application of Cr^{3+} luminescence
310 mapping allowed us to observe the zoning of Mangari corundum by the relative
311 Cr^{3+} content within the mineral lattice (Fig. 2). This method is particularly
312 useful in examining oscillatory zoned corundum from Mangari. Thus lower
313 Cr^{3+} content has been observed in core area subsequently increasing towards
314 the rim. These results correlate with Cr profiles obtained LA-ICP-MS
315 measurements (Fig. 2 and Table 1).

316 The primary and secondary Luc Yen deposits produce transparent crystals
317 with pink areas that have lower Cr concentrations ($\approx 1000 \mu\text{g/g}$) (Fig. 3) than
318 their red areas ($\geq 1500 \mu\text{g/g}$). Such crystals, which are commonly prismatic,
319 have a tendency to form twins (Fig. 3).

320 Our samples of pink sapphires from Morogoro were almost opaque. Their
321 Cr contents are approximately 500 – 700 $\mu\text{g/g}$, with Fe values up to ~ 1200
322 $\mu\text{g/g}$.

323 The blue-violet sapphire samples from the Andranondambo region of
324 Madagascar are transparent with rhombohedral habit and have Fe
325 concentrations of more than 2000 $\mu\text{g/g}$ and Cr content up to 600 $\mu\text{g/g}$ (Table 1).

326 DISCUSSION

327 Changes in chemical composition and in crystal habit (external
328 morphology) occur during *crystal growth* in mineral ontogeny (Grigor'ev,

329 1965). *Alteration* is the next stage in the evolution of single crystals (Grigor'ev,
330 1965). Common alteration processes are crystal deformation (breaking,
331 fragmentation, etc.), chemical effects (dissolution, etching, formation of
332 pseudomorphs etc.), and recrystallization of primary materials (Grigor'ev and
333 Zhabin, 1975). During recrystallization, crystals are “cleaned” as crystal faces
334 are rounded and inclusions resorbed (Grigor'ev and Zhabin, 1975 and
335 references therein). Recrystallization is an important geological process as a
336 determinant of clarity (Grigor'ev, 1965).

337 **Mangari:** Samples from the two Mangari occurrences (Aqua mine and
338 Gitonga pit) had closely similar changes of habit during growth, with similar
339 evolution of their trace element chemistry, Cr concentration in particular, and
340 their color (Figs. 2 and 4). Zoned crystals have shown that habit varied from
341 dipyramidal with white color at the beginning of crystallization under higher P-
342 T conditions, with the most rapid growth of *n* faces ($\text{Cr} \leq 200 \mu\text{g/g}$ by LA-ICP-
343 MS), through pink with dipyramidal faces ($\text{Cr} \approx 700\text{--}1500 \mu\text{g/g}$), to red with
344 prismatic *z* and *c* faces ($\text{Cr} > 1500 \mu\text{g/g}$) growing the most rapidly in the final
345 growth stage at lower pressure and temperature. Zoning in these corundum
346 crystals commonly indicates three growth stages, though either fewer or more
347 may be apparent. Curved boundaries between these zones are caused by
348 dissolution before the start of renewed crystallization with different trace

349 element composition. From observations of specimens from various localities
350 in the area, we conclude that the crystallization of transparent ruby, which took
351 place under granulite facies conditions, occurred late in the polycyclic Pan-
352 African sequence, but that at least one episode of corundum crystallization must
353 have occurred still later (Saul, 2014).

354 **Luc Yen:** Pink zones with lower Cr concentration ($\sim 1000 \mu\text{g/g}$ by EMPA;
355 $\sim 900 \mu\text{g/g}$ by LA-ICP-MS) in rubies from the Luc Yen deposits appear to have
356 had the most rapid growth on their n faces at the beginning of crystallization
357 under higher P-T conditions (Figs. 3 and 4). At $\text{Cr} \geq 1500 \mu\text{g/g}$, the most rapid
358 growth occurred on a faces with a tendency to form twinned crystals. Although
359 fine transparent rubies have been produced from Luc Yen, most crystals are full
360 of defects, including partings along r faces. Color variations from reddish-pink
361 to bright red are typical in these samples (Fig. 3). This color inhomogeneity and
362 the formation of twinned crystals correspond to specific aspects of mineral
363 alteration, infiltration in particular, during recrystallization along cracks and
364 fractures in the calcite marble (see Hoang Quang et al., 1999). In some samples
365 from the Luc Yen secondary deposit, ruby crystals appeared yellowish-red and
366 visually opaque (Fig. 1). Yet after plate preparation, the cores appeared
367 completely transparent with bright red color (Table 1 and Fig. 3). According to
368 the chemical data, Cr concentrations throughout the crystal are above 1500

369 $\mu\text{g/g}$, similar to the Cr concentrations in Luc Yen rubies from primary deposits
370 (Fig. 3). The yellowish-red color of these samples appeared close to the
371 terminating crystal faces where micro-cracks had developed, permitting
372 possible infill by goethite and other iron oxides that might account for the
373 yellowish coloration.

374 **Morogoro:** The Fe concentration (up to about 700 $\mu\text{g/g}$), along with Cr (up
375 to 1200 $\mu\text{g/g}$), in pink sapphires from Morogoro correlate with their
376 dipyrarnidal habit with elongation along the *c* axis. Rim-to-rim measurements
377 (Table 1) showed moderate variations in trace-element concentrations from the
378 beginning of growth (core) to the end (rim). This suggests that these crystals
379 started and continued their growth under similar conditions. Their formation
380 took place under granulite facies conditions (Le Goff et al., 2004) at $P \sim 7.7$
381 kbar and $T \sim 695$ °C (Alter et al., 1982). We observed many partings along *r*
382 crystal faces as evidence of high pressure/temperature conditions during their
383 growth (see Scheuplein and Gibbs, 1960). Neither of our Morogoro specimens,
384 both of which were pink corundum in feldspar-biotite gneiss, had undergone
385 recrystallization.

386 **Andranondambo:** The corundum (sapphires) from Andranondambo have
387 Fe contents above 2000 $\mu\text{g/g}$ with relatively low Cr (~ 600 $\mu\text{g/g}$). Trace-element
388 concentration correlates with a rhombohedral habit with *r* and *a* faces (Fig. 4).

389 This transparent corundum may have been recrystallized, as were the
390 transparent ruby crystals of Luc Yen. In Madagascar, this probably occurred
391 very late along the retrograde metamorphic path in the course of a multistage
392 process (see Rakotondrazafy et al., 2008). Nearly all corundum samples are full
393 of partings along *r* faces caused by the high pressure/temperature conditions
394 during growth (see Scheuplein & Gibbs, 1960).

395 **IMPLICATIONS**

396 Hartman (1962, 1980) proposed that the crystal habit of corundum is not
397 solely determined by crystal structure, but also by environmental factors present
398 during crystal growth. Our data show that during growth with decreasing
399 pressure and temperature, the corundum chemistry changes, and that change
400 correlates with crystal habit (Fig. 4). This correlation may be explained by:

401 1. the direct impact of Fe and Cr trace elements on the different rates at
402 which ions are taken up by different crystal faces during the growth. Such
403 differences alter surface energy relations, and produce changes in crystal habit,
404 as shown for rutile synthesized by the Verneuil process (Grigor'ev and Zhabin,
405 1975);

406 2. the impact of additional factors, which influenced changes in the
407 corundum morphology, such as P, T and pH. With the changing of crystal habit,

408 selective absorption of trace elements by defined faces of corundum crystals
409 may affect continued growth and modifications (Chase, 1966).

410 The ontogeny of naturally-occurring transparent and opaque corundum
411 from five important sources in Kenya, Tanzania, Madagascar, and Vietnam
412 provides insights into their crystal growth in particular geological
413 environments. A range of analytical micro-scale techniques (RS, EMPA and
414 LA-ICP-MS) were applied in examining changes in trace element contents
415 during crystal growth, and their possible effects on crystal shape.

416 The variations in corundum morphology are directly correlated with trace-
417 element content and with varying P-T conditions that prevailed during growth.
418 Dipyramidal habit combined with white color in corundum from Mangari,
419 Kenya, showed Cr concentrations below 700 $\mu\text{g/g}$ and the growing under high
420 P-T conditions. In contrast, prismatic habit with bright red color were linked to
421 Cr concentrations $\geq 1500 \mu\text{g/g}$ in samples from Luc Yen, Vietnam, and those at
422 Mangari that formed under lower P-T. Concentrations of Cr between 700–1500
423 $\mu\text{g/g}$ are related to pink color and combinations of different crystal habits
424 (dipyramidal, prismatic, or dipyramidal-prismatic) in these samples. Contents
425 of Fe $\sim 700 \mu\text{g/g}$ and Cr $\sim 1200 \mu\text{g/g}$ in sapphire crystals from the Morogoro
426 area of Tanzania produced pink color that correlated with dipyramidal habit and
427 elongation along the *c* axis. Rhombohedral habit and blue-violet color were

428 observed at Cr ~500 µg/g and Fe >2000 µg/g in sapphires from
429 Andranondambo in Madagascar, formed during the final stage of contact
430 metamorphism.

431 This study leads the way for further testing of links between trace element
432 concentrations and crystal habits in corundum from other gem corundum
433 deposits.

434

435 **ACKNOWLEDGMENTS**

436 The authors thank the Centre of Gemstones Research of JGU for providing
437 of samples for investigations. The former Director Viktor K. Garanin and
438 colleague Dmitriy I. Belakovsky, Fersman Mineralogical Museum RAS, and
439 Delia Rösel, Freiberg Mining Academy and University of Technology
440 (Germany), provided helpful consultations on the results, which improved the
441 manuscript. The research was supported by the scholarship A-13-00099 of
442 German Academic Exchange Service (DAAD) and the Centre for Gemstones
443 Research of JGU.

444 **REFERENCES CITED**

445 Acharya, R., Burte, P.P., Nair, A., Reddy, A.V.R., and Manohar, S.B. (1997)
446 Multielement analysis of natural ruby samples by neutron activation using

- 447 the single comparator method. *Journal of Radioanalytical and Nuclear*
448 *Chemistry*, 220, 223 – 227
- 449 Alekseev, V.I., and Marin, Yu.B. (2012) Structural and geochemical
450 heterogeneity of natural crystals and microgeochemical line of research in
451 ontogeny of minerals. *Geology of Ore Deposits*, 54, 589 – 601
- 452 Alter, R., Okrusch, M., and Bank, H. (1982) Corundum- and kyanite-bearing
453 anatexites from the Precambrian of Tanzania. *Lithos*, 15, 191 - 197
- 454 Chase, A.B. (1966) Habit modification of corundum crystals grown from
455 molten PbF₂-Bi₂O₃. *Journal of the American Ceramic Society*, 49, 233 -
456 236
- 457 Garnier, V., Ohnenstetter, D., Giuliani, G., Malusci, H., Deloule, E., Phan
458 Vamm, L., and Hoang Quang, V. (2005) Age and significant of ruby-
459 bearing marble from the Red River shear zone, Northern Vietnam. *The*
460 *Canadian Mineralogist*, 43, 1315 – 1329
- 461 Giuliani, G., Ohnenstetter, D., Garnier, V., Fallick, A.E., Rakotondrazafy, M.,
462 and Schwarz, D. (2007) The geology and genesis of gem corundum
463 deposits. In *Geology of gem deposits*, 23 – 78. Ed. by Lee A. Groat.
464 Mineralogical association of Canada, 37
- 465 Grigor'ev, D.P. (1961) *The ontogeny of minerals*, 284 p. University of L'vov
466 publ. (in Russian)

- 467 Grigor'ev, D.P. (1965) The ontogeny of minerals, 250 p. Israel Program for
468 Scientific Translations
- 469 Grigor'ev, D.P., and Zhabin, A.G. (1975) Ontogeny of minerals, 340 p. Nauka
470 publ., Moscow (in Russian)
- 471 Häger, T., and Dung, P.T. (2000) Quantitative Fluoreszenz-Spektroskopie an
472 natürlichen und synthetischen Rubinen. Berichte der Deutschen
473 Mineralogischen Gesellschaft. Beihefte zum European Journal of
474 Mineralogy, 12, Beih. 1:72 (in German)
- 475 Harlow, G.E., and Bender, W. (2013) A study of ruby (corundum) from the
476 Mogok belt, Myanmar, searching for chemical fingerprints. American
477 Mineralogist, 98, 1120 - 1132
- 478 Hartman, P. (1962) The structure morphology of corundum. Zapiski
479 Vsesouznogo Mineralogicheskogo Obshestva (All-Union Mineralogical
480 Society Proceedings), 91, 672 – 682
- 481 Hartman, P. (1980) The attachment energy as a habit controlling factor 3.
482 Application to corundum. Journal of Crystal Growth, 49, 157
- 483 Hazen, R.M., Papineau, D., Bleeker, W., Downs, R.T, Ferry, J.M., McCoy, J.,
484 Sverjensky, D.A., and Yang, H. (2008) Mineral evolution. American
485 Mineralogist, 93, 1693 – 1720

- 486 Hoang Quang, V., Giuliani, G., Phan Trong, T., Coget, P., France-Lanord, Ch.,
487 and Pham Van, L. (1999) Origin of ruby formation in Yen Bay Province.
488 Tap chi Dia Chat, Series B, 13 – 14, 118 – 123
- 489 Hughes, R.W. (1997) Ruby & Sapphire, 512 p. RRWH Publishing, Boulder,
490 CO
- 491 Jochum, K.P., Nohl, U., Herwig, K., Lammel, E., Stoll, B., and Hofmann, A.W.
492 (2005) GeoReM: a new geochemical database for reference materials and
493 isotopic standards, Geostandards and Geoanalytical Research, 29, 333 – 338
- 494 Jochum, K.P., Weis, U., Stoll, B., Kuzmin, D., Yang, Q., Raczek, I., Jacob,
495 D.E., Stracke, A., Birbaum, K., Frick, D.A., Günther, D., and Enzweiler, J.
496 (2011) Determination of reference values for NIST SRM 610-617 glasses
497 following ISO Guidelines. Geostandards and Geoanalytical Research, 35,
498 397 – 429
- 499 Jochum, K.P., Scholz, D., Stoll, B., Weis, U., Wilson, S.A., Yang, Q., Schwalb,
500 A., Brner, N., Jacob, D.E., and Andreae, M.O. (2012) Accurate trace
501 element analysis of speleothems and biogenic calcium carbonates by LA-
502 ICP-MS. Chemical Geology, 318–319, 31–44
- 503 Kane, R.E., McClure, S.F., Kammerling, R.C., Khoa, N.D., Mora, C., Repetto,
504 S., Khai, N.D., and Koivula J.I. (1991) Rubies and fancy sapphires from
505 Vietnam. Gems & Gemology, 27, 136 – 155

- 506 Krivovichev, S.V. (2013) Structural complexity of minerals: information
507 storage and processing in the mineral world. *Mineralogical Magazine*, 77,
508 275 – 326
- 509 Le Goff, E., Deschamps, Y., Muhongo, S., Cocherie, A., Milesi, J.P., Pinna, P.,
510 Msechu, M., and Msihili, A. (2004) The Tanzanian “Ruby Belt”: structural,
511 petrological geochronological constraints within the Pan-African orogeny,
512 p. 259. Examples from the Morogoro and Mahenge Districts. 20th
513 Colloquium of African Geology, Orleans, France
- 514 Le Goff, E., Deschamps, Y., Cocherie, A., Guerrot, C., and Ketto, D. (2008)
515 Structural, petrological and geochronological constraints of the Tanzanian
516 ruby belt, p. 133. 22^{ème} Réunion des Sciences de la Terre Nancy, France
- 517 Mercier, A., Debat, P., and Saul J. (1999) Exotic origin of the ruby deposits of
518 the Mangari area in SE Kenya. *Ore Geology Reviews*, 14, 83 – 104;
- 519 Muhlmeister, S., Fritsch, E., Shigley, J.E., Devouard, B., and Laurs, B.M.
520 (1998) Separating natural and synthetic rubies on the basis of trace-element
521 chemistry. *Gems and Gemology*, 34, 80–101
- 522 Pavlishin, V.I., Yushkin, N.P., and Popov, V.A. (1988) Ontogenetic method in
523 mineralogy, 119 p. Naukova Dumka publ., Kiev (in Russian)

- 524 Pirogov, B.I. (1985) Ontogenetic method in understanding of technological
525 properties of minerals, pp. 22 – 30. In problems of mineral ontogeny.
526 Nauka, L'vov (in Russian)
- 527 Pham Van, L., Hoang Quang, V., Garnier, V., Giuliani, G., and Ohnenstetter, D.
528 (2004) Marble-hosted ruby from Vietnam. *The Canadian gemmologist*, 25,
529 83-95
- 530 Popov, V.A. (1984) Practical crystal morphology of minerals, 190 p.
531 Sverdlovsk: Academy of Sciences USSR (in Russian)
- 532 Prieto, M., Putnis, A., Arribas, J., and Fernandez-Diaz, L. (1992) Ontogeny of
533 barite crystals grown in a porous medium. *Mineralogical Magazine*, 56, 587
534 – 598
- 535 Rakotondrazafy, A.F.M., Moine, B., and Cuney, M. (1996) Mode of formation
536 of hibonite ($\text{CaAl}_{12}\text{O}_{19}$) within the U-Th skarns from the granulites of S-E
537 Madagascar. *Contributions to Mineralogy and Petrology*, 123, 190 – 201
- 538 Rakotondrazafy, A.F.M., Giuliani, G., Ohnenstetter, D., Fallick, A.E.,
539 Rakotosamizany, S., Andriamamonjy, A., Ralantoarison, Th.,
540 Razanatseho, M., Offant, Y., Garnier, V., Maluski, H., Dunagre, Ch.,
541 Schwarz, D., and Ratrio, V. (2008) Gem corundum deposits of
542 Madagascar: A review. *Ore Geology Reviews*, 34, 134 – 154

- 543 Saul, J.M. (2014) A geologist speculates: on gemstones, origin of gas and oil,
544 moonlike impact scars on the Earth, the emergence of animals and cancer,
545 149 p. Paris: Les 3 Colonnes
- 546 Scheuplein, R., and Gibbs, P. (1960) Surface structure in corundum: I, etching
547 of dislocations. *Journal of the American Ceramic Society*, 43, 458 – 472
- 548 Self, C.A., and Hill, C.A. (2003) How speleotherms grow: An introduction to
549 ontogeny of cave minerals. *Journal of Cave and Karst Studies*, 65, 130 - 151
- 550 Simonet, C. (2000) Géologie des gisements de saphir et de rubis— L'exemple
551 de la John Saul Ruby Mine, Mangare, Kenya, 349 p. Unpublished Ph.D.
552 thesis, University of Nantes, France
- 553 Simonet, C., Fritsch, E., and Lasnier, B. (2008) A classification of gem
554 corundum deposits aimed towards gem exploration. *Ore Geology Reviews*,
555 34, 127–133
- 556 Sorokina, E.S. (2011). Ontogeny and quality of gem ruby from the deposits of
557 Central and South-East Asia, 128 p. Unpublished Ph.D. thesis, Fedorovsky
558 All-Russian Research Institute of Mineral Resources, Moscow, Russia (in
559 Russian)
- 560 Sorokina, E.S., Ozhogina, E.G., Jacob, D.E., and Hofmeister, W. (2012) Some
561 features of corundum ontogeny and the quality of ruby from Snezhnoe
562 deposit, Tajikistan (the Eastern Pamirs). *Zapiski Rossiiskogo*

- 563 Mineralogicheskogo Obshchestva (Proceedings of the Russian
564 Mineralogical Society), 141,100–108 (in Russian)
- 565 Stenonis, N. (1669) De solido intra solidum naturaliter contento dissertationis
566 prodromus. Florentie: Ex Typographia sub Signo Stellæ (in Latin)
- 567 Sunagawa, I. (2003) Growth histories of mineral crystals as seen from their
568 morphological features. Crystal growth technology, pp. 1 – 23. Ed. by
569 Byrappa, K. & Ohachi, T.N.Y.: William Andrew Pub.; Berlin; N.Y.:
570 Springer
- 571 Upton, B.G.J., Hinton, R.W., Aspen, P., Finch, A., and Valley, J.W. (1999)
572 Megacrysts and associated xenoliths: evidence for migration of
573 geochemically enriched melts in the uppermost mantle beneath Scotland.
574 Journal of Petrology, 40, 935 - 956
- 575 Yushkin, N.P. (1977) Theory and methods of mineralogy, 291 p. Nauka publ.,
576 L'vov (in Russian)
- 577 Yushkin, N.P. (1985) Genetic methods of mineralogy and ontogeny of
578 minerals, pp. 3 - 9. In problems of mineral ontogeny. Nauka, L'vov (in
579 Russian)
- 580 Zaw, K., Sutherland, L., Yoi, T-F., Meffe, S., and Thu, K. (2015) Vanadium-
581 rich ruby and sapphire within Mogok Gemfield, Myanmar: Implications for
582 gem-color and genesis. Mineralium Deposita, 50, 25–39.

583 Zhabin, A.G. (1979) Ontogeny of minerals, 276 p. Aggregates. Nauka publ.,
584 Moscow (in Russian)
585

586 Fig. 1. Photographs of samples used in this study: A) ruby crystals in calcite
587 marble matrix, Luc Yen, Vietnam (sample size 10.0 x 13.4 cm); B) ruby-
588 bearing rock from a secondary deposit near Luc Yen, Vietnam (sample size
589 10.0 x 14.5 cm); C) sapphire-bearing skarn from Andranondambo, Madagascar
590 (size of the largest blue sapphire crystal is 1.6 x 2.3 cm); D) ruby crystals from
591 Gitonga pit, John Saul mine, Mangari, Kenya (sizes of intermediate crystals
592 from left to right are 1.8 x 1.8 cm, 1.8 x 1.4 cm and 2.0 x 1.5 cm); E) ruby-
593 bearing rock from the Aqua mine, Mangari, Kenya (sizes of ruby crystals are
594 0.8 x 0.5 cm and 0.3 x 0.4 cm); F) corundum crystals in K-feldspar-biotite
595 gneiss from the Morogoro area, Tanzania (sizes of sapphire crystals are 0.9 x
596 2.0 cm and 0.6 x 3.0 cm). Photographs by Elena S. Sorokina.

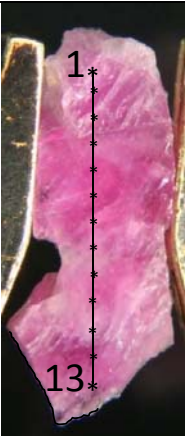

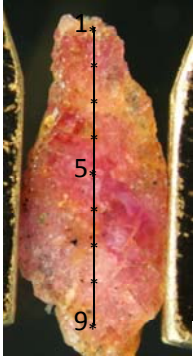
597 Fig. 2. Photomicrographs of corundums from the Gitonga pit (A; magnification
598 is 12x) and the Aqua mine (D; magnification is 8x) in Kenya with oscillatory
599 zonation traced along the growth lines (marked by dotted lines) parallel to *n*
600 face in the core and *z* face in the rim, samples cut parallel to the *c* axis; their RS
601 Cr³⁺ luminescence maps (B and F) and rim-to-rim Cr, V and Ga LA-ICP-MS
602 scans with corresponding colors (C and G; dots represent the locations of
603 measured spots from Table 1).

604 Fig. 3. Photomicrographs of corundums from primary (A; magnification is 6x)
605 and secondary (C; magnification is 10x) Luc Yen deposits in Vietnam with

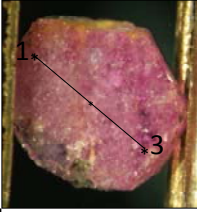
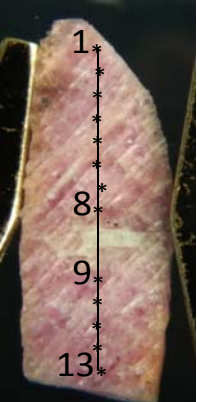
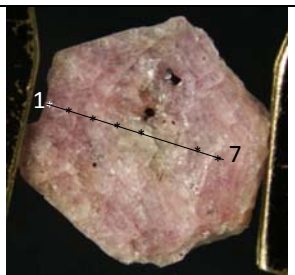
606 parting traced along the growth lines (marked by dotted lines) parallel to n and
607 c faces in the core and the r face in the rim, samples cut parallel to the c axis; B.
608 and D. their EMPA rim-to-rim chemical profiles of Cr, Ti, V, Ga and Fe with
609 corresponding colors (dots represent the locations of measured spots from
610 Table 1).

611 Fig. 4. Diagram showing the correlation between the crystal habit (and color) of
612 corundum from primary and secondary deposits at Luc Yen in Vietnam, the
613 Mangari area of Kenya (Gitonga pit of the John Saul ruby mine, and the Aqua
614 mine), and Morogoro area in Tanzania with PT-parameters of the growth
615 environment, the X axis representing the contents of Fe ($\mu\text{g/g}$) and Y axis is Cr
616 values ($\mu\text{g/g}$).

**Rim-to-rim EMPA (top values) and LA-ICP-MS (bottom values)
measurements ($\mu\text{g/g}$) of representative corundum samples**

Occurrence	Picture of samples with location of spots	Habit	Spacing of spots	N ^o of spot	Ti	V	Ga	Fe	Cr	Mg
Luc Yen, Vietnam	 Plate c axis, magnified 6x	Elongate-prismatic with <i>z</i> , <i>n</i> , <i>c</i> and <i>r</i> faces	930 μm	1	bdl ¹	bdl	bdl	72	1182	bdl
					22	34	75	1240	13	
				2	bdl	bdl	bdl	bdl	1048	bdl
					bdl	30	92	880	19	
				3	bdl	bdl	bdl	bdl	1128	bdl
					427	91	109	983	bdl	
				4	bdl	bdl	bdl	bdl	1143	bdl
					281	58	77	836	18	
				5	bdl	bdl	bdl	bdl	1777	bdl
					bdl	40	74	1519	bdl	
				6	bdl	bdl	bdl	bdl	1841	bdl
					bdl	44	83	1532	20	
				7	bdl	dbl	bdl	bdl	1651	bdl
	71	45	78	1492	bdl					
8	bdl	bdl	bdl	85	1913	bdl				
	27	48	66	1949	257					
9	bdl	bdl	bdl	bdl	1904	bdl				
	bdl	42	67	1367	bdl					
10	84	bdl	bdl	bdl	1253	bdl				
	654	98	93	1455	35					
11	bdl	bdl	bdl	bdl	1069	bdl				
	553	86	88	1367	40					
12	bdl	bdl	bdl	bdl	1856	bdl				
	136	79	85	1639	bdl					
13	bdl	bdl	bdl	bdl	1149	bdl				
	30	30	73	1020	14					
	 Plate \perp c axis magnified 1,6x		880 μm	1	bdl	bdl	bdl	bdl	3228	bdl
					76	39	79	3832	35	
				2	bdl	bdl	bdl	bdl	1926	bdl
					65	58	89	1854	65	
				3	bdl	bdl	bdl	bdl	1091	bdl
					26	49	86	1634	13	
Luc Yen (secondary), Vietnam	 Plate c axis, magnified 10x	Elongate-prismatic with <i>z</i> , <i>n</i> , <i>c</i> and <i>r</i> faces	960 μm	1	bdl	bdl	bdl	167	1290	bdl
					-	-	-	-	-	-
				2	bdl	bdl	164	194	1685	bdl
					-	-	-	-	-	-
				3	bdl	bdl	132	103	978	bdl
					-	-	-	-	-	-
				4	bdl	bdl	bdl	236	2471	bdl
					-	-	-	-	-	-
				5	bdl	135	bdl	140	2474	bdl
					bdl	37	63	1809	bdl	

¹ bdl -measurement below the detection limit

Occurrence	Picture of samples with location of spots	Habit	Spacing of spots	N ^o of spot	Ti	V	Ga	Fe	Cr	Mg
Luc Yen (secondary), Vietnam			1080 μ m	6	bdl	bdl	bdl	230	4055	bdl
				7	bdl	bdl	bdl	131	1235	bdl
				8	bdl	bdl	bdl	227	2454	bdl
				9	bdl	bdl	bdl	186	3369	bdl
				1	bdl	bdl	bdl	774	bdl	
				2	bdl	bdl	bdl	125	1052	bdl
				3	bdl	bdl	174	148	4451	bdl
				1	bdl	bdl	bdl	431	788	bdl
				2	bdl	bdl	bdl	468	749	bdl
				3	bdl	bdl	bdl	473	1040	bdl
				4	bdl	bdl	bdl	486	778	bdl
				5	bdl	bdl	bdl	476	1017	bdl
				6	bdl	bdl	bdl	620	883	bdl
7	bdl	bdl	bdl	665	896	bdl				
8	bdl	bdl	bdl	729	940	bdl				
9	bdl	bdl	bdl	691	1084	bdl				
10	bdl	bdl	bdl	690	944	bdl				
11	bdl	bdl	bdl	511	924	bdl				
12	bdl	bdl	bdl	393	855	bdl				
13	bdl	bdl	bdl	531	910	bdl				
Morogoro, Tanzania		Elongate dipyramidal with c and ω faces	870 μ m	1	bdl	bdl	bdl	431	788	bdl
				2	bdl	bdl	bdl	468	749	bdl
				3	bdl	bdl	bdl	473	1040	bdl
				4	bdl	bdl	bdl	486	778	bdl
				5	bdl	bdl	bdl	476	1017	bdl
				6	bdl	bdl	bdl	620	883	bdl
				7	bdl	bdl	bdl	665	896	bdl
				8	bdl	bdl	bdl	729	940	bdl
				9	bdl	bdl	bdl	691	1084	bdl
				10	bdl	bdl	bdl	690	944	bdl
				11	bdl	bdl	bdl	511	924	bdl
				12	bdl	bdl	bdl	393	855	bdl
				13	bdl	bdl	bdl	531	910	bdl
			860 μ m	1	bdl	bdl	bdl	669	649	bdl
				2	bdl	bdl	bdl	623	809	bdl
				3	bdl	bdl	bdl	592	926	bdl
				4	bdl	bdl	bdl	484	687	bdl
				1	bdl	bdl	bdl	774	bdl	
				2	bdl	bdl	bdl	125	1052	bdl
				3	bdl	bdl	174	148	4451	bdl
				1	bdl	bdl	bdl	431	788	bdl
				2	bdl	bdl	bdl	468	749	bdl
				3	bdl	bdl	bdl	473	1040	bdl
				4	bdl	bdl	bdl	486	778	bdl
				5	bdl	bdl	bdl	476	1017	bdl
				6	bdl	bdl	bdl	620	883	bdl
7	bdl	bdl	bdl	665	896	bdl				
8	bdl	bdl	bdl	729	940	bdl				
9	bdl	bdl	bdl	691	1084	bdl				
10	bdl	bdl	bdl	690	944	bdl				
11	bdl	bdl	bdl	511	924	bdl				
12	bdl	bdl	bdl	393	855	bdl				
13	bdl	bdl	bdl	531	910	bdl				

Occurrence	Picture of samples with location of spots	Habit	Spacing of spots	N _o of spot	Ti	V	Ga	Fe	Cr	Mg
				5	bdl	bdl	bdl	639	753	bdl
					40	39	101		646	29
				6	bdl	bdl	bdl	653	872	bdl
					bdl	38	93		585	25
				7	bdl	bdl	bdl	557	706	bdl
					40	36	97		586	32
			820 μ m	1	540	bdl	266	bdl	793	bdl
					611	14	226		1002	63
				2	251	bdl	319	bdl	803	bdl
					4160	26	273		629	402
				3	bdl	bdl	333	bdl	539	bdl
					990	21	219		397	88
				4	bdl	bdl	379	bdl	1333	bdl
					887	14	230		830	170
				5	bdl	bdl	282	bdl	3080	bdl
					349	17	228		1713	170
				6	bdl	bdl	321	bdl	3767	bdl
					383	20	242		2117	130
				7	212	bdl	256	bdl	1166	bdl
					461	13	215		1068	136
				8	bdl	bdl	277	bdl	1446	bdl
					338	13	224		1298	124
				9	bdl	bdl	204	bdl	2786	bdl
					129	14	134		1946	155
			870 μ m	1	bdl	bdl	289	bdl	558	bdl
					811	17	279		476	136
				2	bdl	bdl	175	122	346	bdl
					743	15	251		331	86
				3	487	bdl	484	135	570	bdl
					784	19	290		422	143
				4	bdl	bdl	318	bdl	495	bdl
					1334	18	271		426	173
				5	bdl	bdl	259	bdl	441	bdl
					1039	16	240		282	212
				6	bdl	bdl	257	bdl	385	bdl
					886	14	243		336	145
				7	bdl	bdl	344	bdl	664	bdl
					610	17	276		348	99
				8	bdl	bdl	284	bdl	523	bdl
					762	14	231		378	576
				9	bdl	bdl	183	bdl	913	bdl
					201	14	231		475	89
				10	bdl	bdl	270	bdl	827	bdl
					928	16	247		742	171

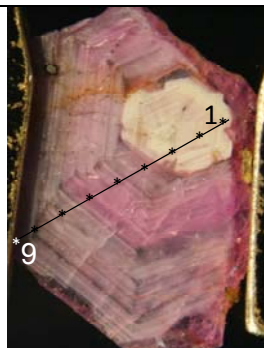


Plate \perp c axis, magnified 10x

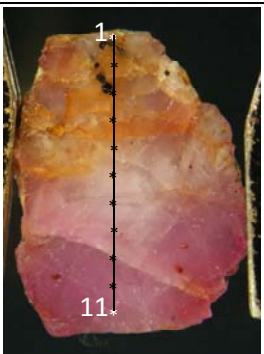


Plate \parallel c axis, magnified 8x

Rim is elongate-prismatic with z , ω , n , c and r faces, core and intermediate area are dipyrarnidal

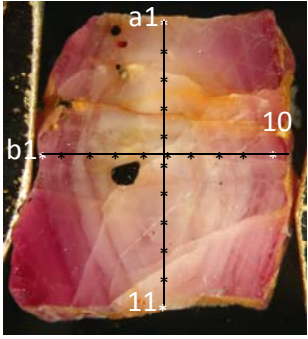
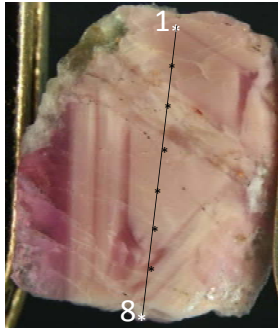
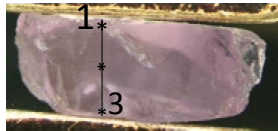
Gitonga pit, Kenya

623

624

625

626

Occurrence	Picture of samples with location of spots	Habit	Spacing of spots	N ^o of spot	Ti	V	Ga	Fe	Cr	Mg
Gitonga pit, Kenya	 <p>Plate c axis, magnified 8x</p>	Rim is elongate-prismatic with <i>z</i> , <i>ω</i> , <i>n</i> , <i>c</i> and <i>r</i> faces, core and intermediate area are dipyrarnidal	870 μm	11	bdl	bdl	236	bdl	931	bdl
					293	14	213		569	118
			830 μm – “a” profile by EMPA	1	bdl	bdl	319	bdl	533	bdl
			2	bdl	bdl	391	bdl	452	bdl	
			3	bdl	bdl	316	bdl	572	bdl	
			4	bdl	bdl	341	bdl	543	bdl	
			5	bdl	bdl	263	bdl	454	bdl	
			6	bdl	bdl	283	bdl	694	bdl	
			7	bdl	bdl	373	bdl	bdl	bdl	
			8	bdl	bdl	317	bdl	246	bdl	
			9	bdl	bdl	294	bdl	429	bdl	
10	bdl	bdl	300	bdl	422	bdl				
11	bdl	bdl	162	109	405	bdl				
Aqua mine, Kenya	 <p>Plate c axis, magnified 12x</p>	Rim is elongate-prismatic with <i>z</i> , <i>ω</i> , <i>n</i> , <i>c</i> and <i>r</i> faces, core and intermediate area are dipyrarnidal	800 μm	1	834	bdl	bdl	bdl	1378	bdl
					712	18	152		1206	160
			2	bdl	bdl	bdl	bdl	1439	bdl	
					4965	35	210		1508	374
			3	160	bdl	236	bdl	1106	bdl	
					3128	36	185		1041	141
			4	bdl	bdl	333	105	1253	bdl	
					2128	27	203		823	114
			5	bdl	bdl	251	bdl	918	bdl	
					6876	30	212		912	698
6	1995	bdl	275	bdl	1654	bdl				
		1593	29	195		1125	41			
7	bdl	bdl	203	bdl	1286	bdl				
		5266	31	215		976	815			
8	bdl	bdl	362	bdl	1003	bdl				
		3228	27	187		1032	239			
Andranondambo	 <p>Plate c axis, magnified 12x</p>	Rhombohedral for blue-violet crystals with <i>r</i> and <i>a</i> faces	1000 μm	1	bdl	bdl	bdl	2473	bdl	bdl
					148	9	29		243	75
			2	bdl	bdl	bdl	2621	bdl	bdl	
					150	12	42		301	81
3	bdl	bdl	bdl	2422	bdl	bdl				
		290	10	24		607	71			

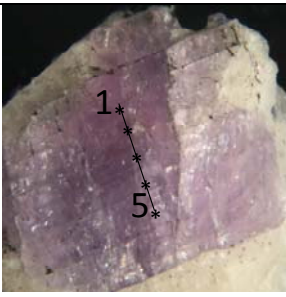
Occurrence	Picture of samples with location of spots	Habit	Spacing of spots	N ^o of spot	Ti	V	Ga	Fe	Cr	Mg
Andranondambo, Madagascar	 <p>Plate $\perp r$ face, magnified 2x</p>	intergrown with calcite	1100 μm	1	bdl	bdl	bdl	2738	332	bdl
					152	11	42		343	98
				2	bdl	bdl	bdl	2648	455	bdl
					165	10	38		315	111
				3	bdl	bdl	bdl	3014	330	bdl
					537	11	34		230	82
				4	bdl	bdl	bdl	2901	591	bdl
					88	7	32		149	60
				5	bdl	bdl	bdl	2532	223	bdl
					81	7	33		bdl	46

Figure 1



Figure 2

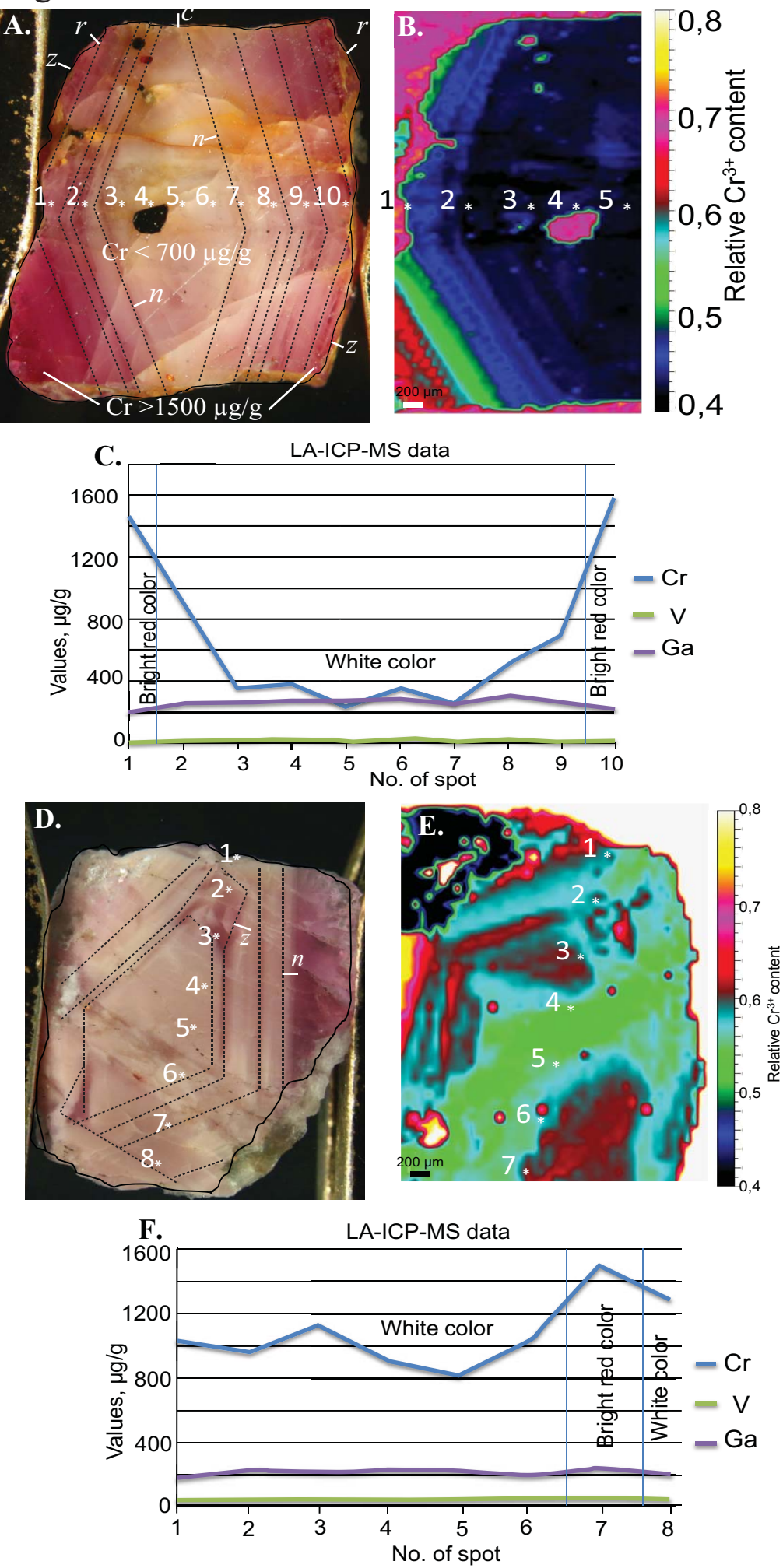


Figure 3

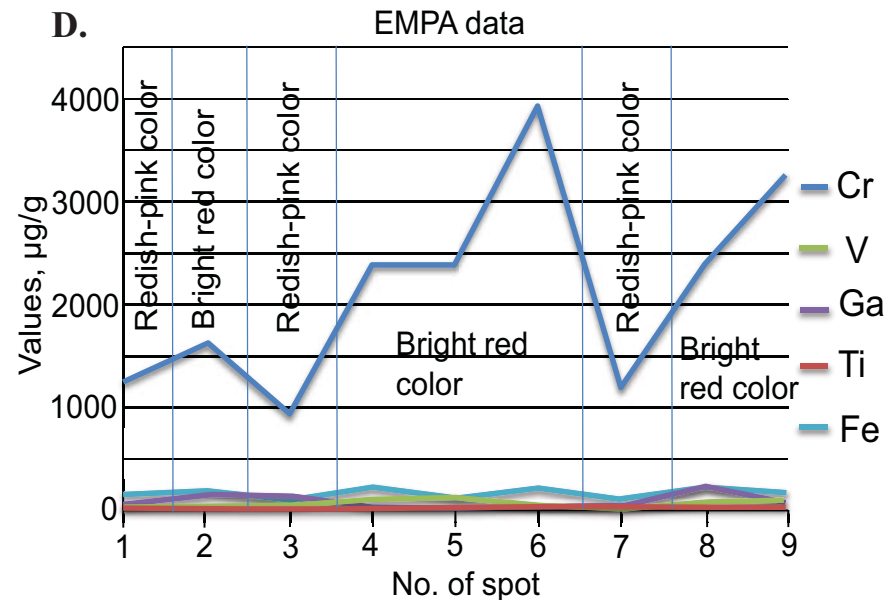
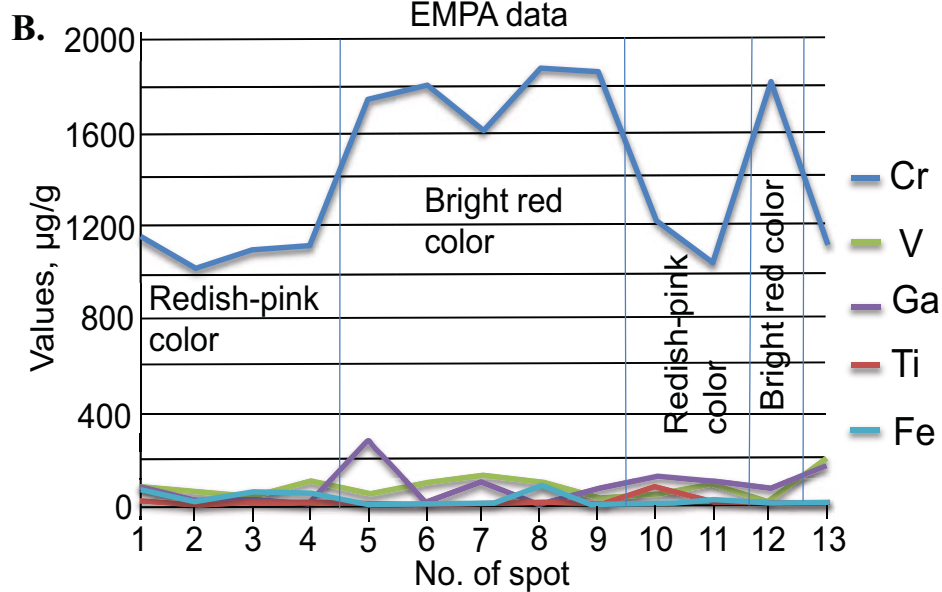
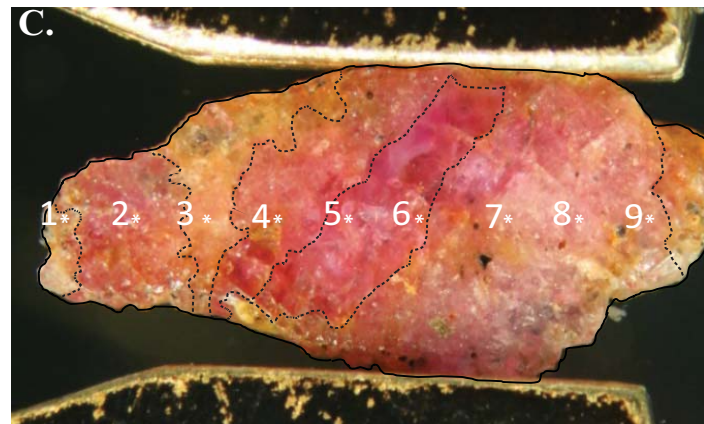
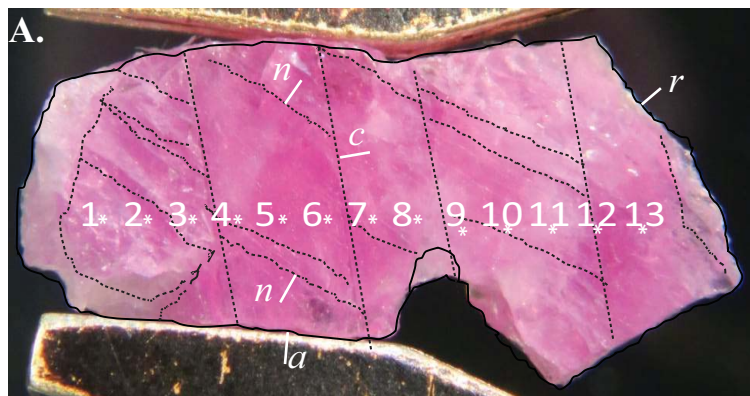


Figure 4

